Traceable measurement of nanoparticle size using a scanning electron microscope in transmission mode (TSEM)

Meas. Sci. Technol. **22** (2011) 094002 (9pp) doi:10.1088/0957-0233/22/9/094002

Traceable measurement of nanoparticle size using a scanning electron microscope in transmission mode (TSEM)

T Klein, E Buhr, K-P Johnsen and C G Frase

Physikalisch-Technische Bundesanstalt, Bundesallee 100, 38116 Braunschweig, Germany

E-mail: Tobias.Klein@ptb.de

Received 9 January 2011, in final form 3 March 2011
Published 8 August 2011
Online at stacks.iop.org/MST/22/094002

Abstract
Traceable size measurements of nanoparticles are accomplished by means of a calibrated scanning electron microscope operated in transmission mode (TSEM). An image analysis tool was developed which individually determines the boundary and size of every particle based on modelled TSEM signals obtained by Monte Carlo simulations. The model relies on first-principle electron scattering theory taking into account particle and instrument properties. A series of TSEM images containing thousands of particles can be analysed in automated batch processing to attain a particle size distribution. As examples, nanoparticles of three different material classes (gold, silica, latex) with sizes ranging from about 5 to 60 nm are analysed. An uncertainty analysis reveals expanded measurement uncertainties (95% confidence interval) of the mean diameter in the range of 1 to 3 nm.

Keywords: nanoparticle size, TSEM, STEM-in-SEM, Monte Carlo simulation, image analysis

1. Introduction

Nanoparticles generate a lot of interest in both fundamental and applied science due to their size-dependent features which promise new physical effects and improved consumer goods. On the other hand, increased usage of nanoparticles in everyday products leads to questions and concerns regarding health, safety and environmental issues. Addressing these questions requires accurate size measurements in order to analyse cause–effect relationships. In turn accurate and traceable measurements assist the exploitation of the unique features of nanoparticles.

While ensemble techniques such as dynamic light scattering (DLS) or small angle x-ray scattering (SAXS) probe a large number of nanoparticles, at the same time their findings are calculated from the direct measurand (e.g. intensity) using model assumptions such as spherical particle shape, log-normal size distributions, etc. Compared to ensemble measurements, microscopic imaging techniques such as scanning electron microscopy (SEM) measure every single probed particle and can thus individually assess e.g. particle size and shape. However, when accurate particle size distributions are of interest, these techniques may lack statistical accuracy since often only a limited number of particles can be measured in practice. Automatic batch imaging and processing may improve this situation, especially if the analysed nanoparticles have a narrow size distribution like, e.g., most reference materials.

Aiming for traceable measurements of nano-objects, a special SEM technique using a transmission electron detector (TSEM) is a promising candidate: imaging of atomic lattice fringes as well as traceable measurements of membrane masks could be demonstrated [1, 2]. Furthermore, the feasibility of the technique for nanoparticle measurements has been shown [3]. Compared to secondary electron imaging often used in SEM, TSEM measurements exhibit a number of advantages such as improved resolution and decreased sensitivity regarding specimen charging. Moreover, accurate simulation of TSEM image formation is less complex than comparable simulations of secondary electron imaging [4]. These advantages may be exploited for an improved localization of particle boundaries.

We report on new traceable TSEM measurements of metal, ceramic and polymer particles in the size range from

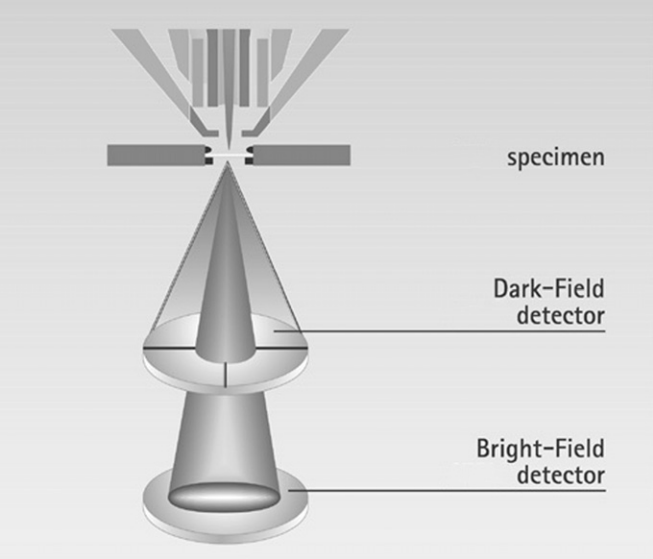

Figure 1. Schematic drawing of the transmission detector capable of dark-field and bright-field imaging, by courtesy of Zeiss.

5 to 60 nm. Four steps have to be taken on the route to accurate nanoparticle size measurements traceable to the SI unit 'metre': the distance between two sampling points (the 'pixel size' in SEM images) has to be known exactly (section 2), a reliable criterion to determine the particle boundary from its image is needed (section 3), a sufficient number of measurements for statistically meaningful results has to be ensured (section 4), and finally, an uncertainty budget for the particle size needs to be established (section 5).

2. Experimental details

2.1. Instrumentation

The experimental setup has been described in detail in [3]. In short, particle samples are analysed using a standard SEM (Zeiss Supra 35 VP) equipped with a transmission detector readily available as an add-on. The detector consists of five solid-state electron detectors, four of which are used as dark-field detectors, see figure 1. The fifth detector placed underneath a small pinhole is used for bright-field imaging. It records electrons which pass through the specimen without appreciable deflection. For the setup used in this study the aperture half-angle of the bright-field detector is 16 mrad. To speed up image acquisition and to minimize operator bias automatic image acquisition has been developed based on processing a list of non-overlapping measurement positions. All images were acquired in the bright-field imaging mode and stored as 16-bit files.

2.2. Calibration of pixel size

To determine the pixel size we calibrated the instrument using a 2D grating with a nominal grating pitch of 144 nm consisting of aluminium bumps on silica (150-2D from Advanced Surface Microscopy Inc.), see figure 2. The actual pitch in the x and y directions was calibrated in our lab using a deep UV

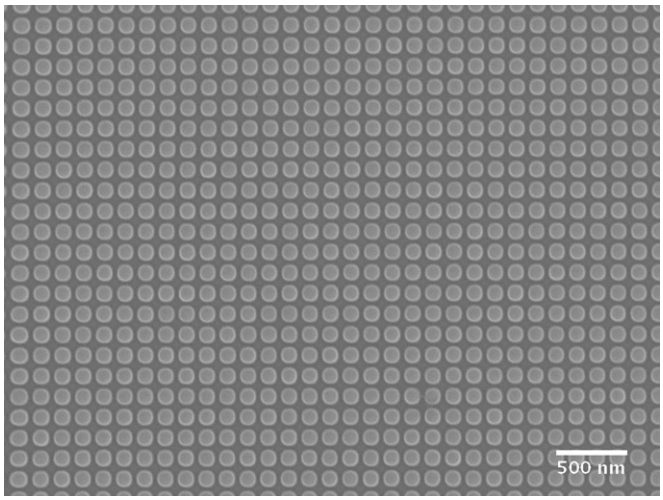

Figure 2. Typical SEM image of the 2D grating with a mean pitch of 144 nm used for calibration.

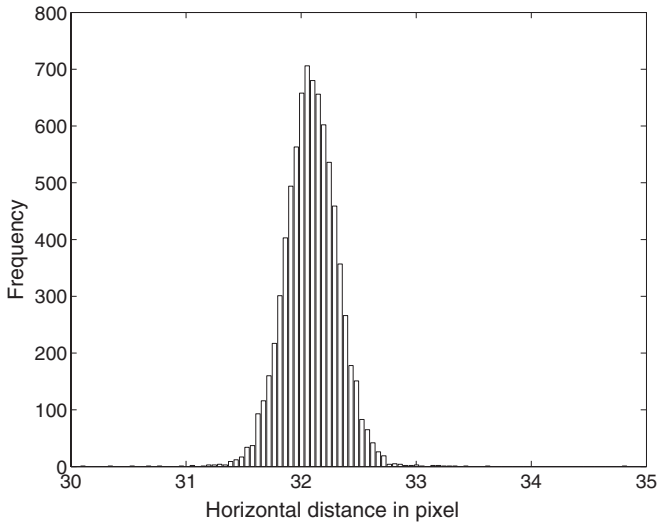

Figure 3. Distribution of measured horizontal distances (in pixel units) between adjacent aluminium bumps of the calibration standard, shown here for 25 000-fold magnification.

laser diffractometer which yields traceable values for the mean grating pitch [5, 6].

During calibration and measurement the same SEM parameters are used, i.e. 30 kV acceleration voltage, 3.0 mm working distance, same magnification settings (between 25 000-fold and 150 000-fold referring to standard polaroid size), same scan speed of the electron beam, etc. Since electron microscopy measures individual distances between adjacent grating elements, a large number of individual pitch values have to be measured across the grating to determine mean pitch values with sufficient accuracy. As an example, figure 3 shows the distribution of pitch values obtained for 25 000-fold magnification. The spread of pitch values is mainly due to a variation of the position of individual Al bumps on the grating. Measurements were carried out at different spots on the grating revealing sufficient homogeneity of the mean pitch across the grating.

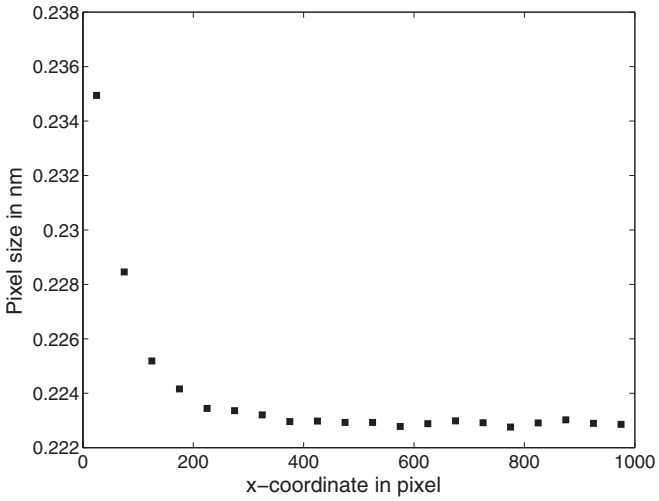

Figure 4. Pixel size in the *x* direction as a function of the position in the digital image: due to the effect of 'leading edge distortion' the pixel size at the beginning of the scan deviates from the rest of the image.

The calibration efforts lay open some points to consider when accurate size measurements with an SEM are desired: the pixel size in the *x* and *y* directions differs by some tenths of a per cent. Moreover, the reproducibility of pitch measurements in the *y* direction is inferior compared to that in the *x* direction which may be attributed to the fact that the electron beam has to be repositioned in the *y* direction after every line scan. Another issue shown in figure 4 is the so-called leading edge distortion, a systematic deviation of the pixel size at the beginning of the line scan due to the initial acceleration of the electron beam along the *x* axis (line scan direction). Therefore, for both calibration and measurement, the first 200 of the 1024 pixels along the scanning direction are omitted.

2.3. Sample preparation

We studied gold reference particles (NIST RM 8011, nominal diameter 10 nm), silica particles used for quality control (IRMM 304, quoted hydrodynamic diameter from DLS measurements about 40 nm) and latex spheres (Duke Scientific, nominal diameter 50 nm). The particles are delivered in suspension. For the measurements, the particles are deposited on usual TEM grids which consist of a thin carbon film supported by a copper grid. For the latex particles nickel grids are used. Sample preparation takes place under clean room conditions. TEM grids are placed in the moulds of a Teflon plate and one drop of undiluted suspension is placed on every grid using a syringe. The samples are then kept for different times ranging from a few minutes to a couple of hours in an atmosphere with saturated water content to avoid evaporation of the liquid. Subsequently the droplet is removed by a piece of clean room tissue ensuring the suspension is completely removed. After fixing the samples to a multi TEM grid holder they are ready for TSEM examination.

3. Simulation and threshold determination

In the evaluation of the TSEM images of nanoparticles a precise determination of the particle boundary is essential for accurate size measurements. A convenient and often used method to determine the particle boundary in electron microscopy images is the application of a global threshold level. Diverse thresholding algorithms are available and may be applied to separate particles from the background [7]. However, depending on the chosen algorithm, the resulting size distributions may differ significantly [8]. Conventional thresholding algorithms exclusively make use of the grey scale values of the image under test and neglect the particular physical effects involved in image formation. Boundary detection and thus particle size analysis may be improved if the physical process of image formation is considered for thresholding. In the case of SEM the image formation process can be conveniently modelled using Monte Carlo simulations [9].

We applied the versatile Monte Carlo simulation program package 'MCSEM' (Monte Carlo simulation of electron microscopy) which has been developed by some of the authors [10]. This simulation program enables a thorough and realistic modelling of SEM images taking into account all relevant parameters that may influence image formation. The desired measurement quantities may thus be determined from the experimental images by quantitative comparison with the simulated ones. In our studies we determine the position of the particle boundary and finally the particle size.

A key feature of the simulation tool MCSEM is its modular design. There are different program modules available for different aspects of the simulation, i.e. form of the electron probe, specimen topography, probe–sample interaction and electron detection. The modules can easily be replaced or enhanced to adapt the program to new simulation tasks. Different shapes of the electron beam can be modelled (conical or parallel, Gaussian distribution or non-Gaussian). Various specimen topography modules are available ranging from simple layer structures to complex 3D structures, offering a flexible system of specimen definition. Complex 3D structures are composed of basic geometric bodies and are defined by a simple script language. The core module simulates electron diffusion in solid state: elastic scattering is based on tabulated Mott scattering cross-sections [11] while inelastic scattering is modelled by a modification of the Bethe continuous slowing down approximation [12]. Electron detectors with different properties can be simulated for backscattered, secondary and transmitted electrons. Further details of MCSEM can be found in [10].

The quality of simulation results depends on the accuracy of the input parameters used in the simulation. Therefore it is worthwhile to undertake some effort to determine these parameters specifically for the conditions present in the experimental setup: due to an aperture in the beam path the incoming electron beam is conical. Its Gaussian beam profile can be verified by the signal profile across a heavy nano-object acting as an almost ideal aperture. All incoming electrons are assumed to have the same energy because a

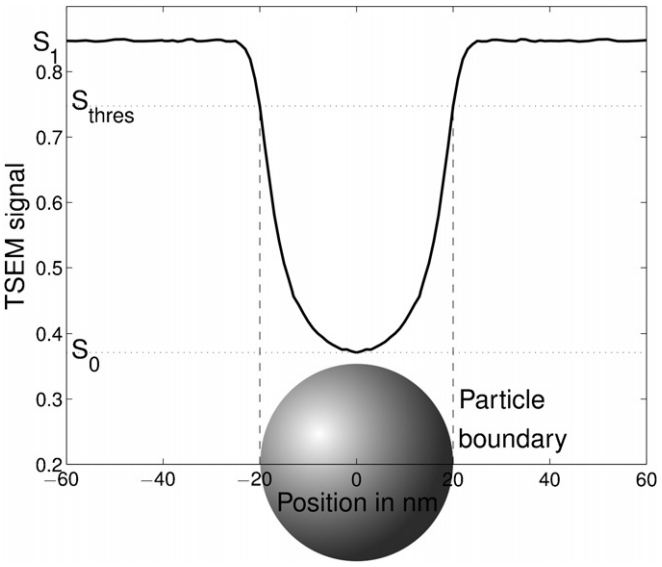

Figure 5. Simulated signal profile across a 40 nm silica sphere on a carbon support film. Since the diameter of the sphere assumed in the simulation is known, the signal level S_{thres} at its boundary can easily be determined.

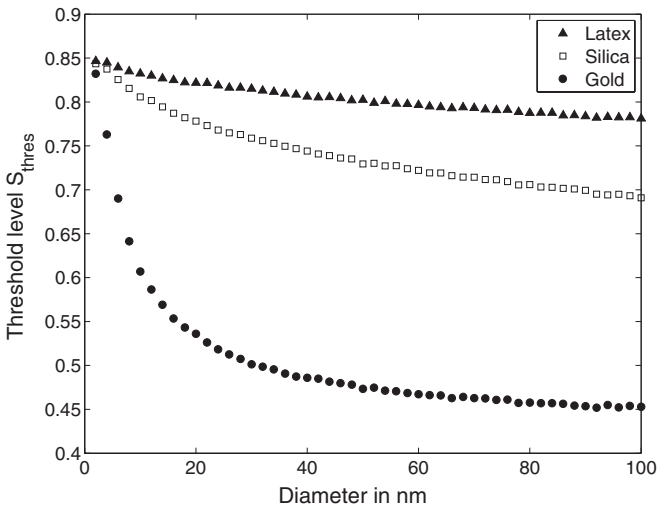

Figure 6. Signal level at the particle boundary as a function of the particle diameter for the three materials present in this study.

field emission gun is used. The acceptance solid angle of the transmission electron detector is deduced from the geometry of its aperture and its position relative to the sample. The energy sensitivity of the detector can be determined experimentally. The nanoparticles are assumed to be spherical and to consist of a homogeneous material. The thickness of the carbon support film on which the particles are located is stated by the manufacturer together with its range of variation. Despite the effort put into the determination of the parameters, they can only be specified within certain limits. The uncertainties attributed to the various input parameters finally lead to corresponding uncertainties of the simulation results which have to be accounted for in the overall uncertainty analysis, see section 5.

As an example, figure 5 shows the simulated TSEM signal profile of a silica sphere with a size of 40 nm on a 12.5 nm carbon film. The signal level outside the particle S_1 is reduced to 85% due to scattering processes in the carbon film leading to deflections sufficient to miss the bright-field detector. In the centre of the particle the signal reaches its minimum S_0. Since a certain portion of the incoming electrons pass the particle and hit the detector, the minimum signal level is larger than zero. The signal level at the boundary position is called the threshold signal level S_{thres}.

The threshold level S_{thres} depends on both particle size and material as can be seen in figure 6. The dependence on material is due to different scattering properties, e.g. gold particles with high atomic number scatter electrons much more strongly than less dense latex particles. The decrease of the threshold level with increasing particle size can be understood as follows: assuming an infinitely thin electron beam just touching the particle, the signal level at the particle boundary is the same as the signal level outside the particle. A broader electron beam leads to the situation that about 50% of the incoming electrons run alongside the particle without interacting. This portion, again reduced by the carbon support film, corresponds to a signal level of about 43% (i.e. half of 85%). The second half of the electrons enter the particle and possibly undergo scattering events and may thus miss the transmission detector. Since the probability of a scattering event becomes larger for a larger interaction length, i.e. for larger particles, the portion of electrons that pass through the particle and hit the detector decreases with increasing particle size. Hence, the signal level at the particle boundary becomes smaller for larger particles. In the limiting case of very large particles, almost all electrons that enter the particle are scattered and hence do not contribute to the detector signal. Only the portion of electrons that run alongside the particle is detected, resulting in a threshold level of about 43%. In figure 6 this asymptotical progression can be seen for gold while for silica and latex the convergence occurs at larger sizes.

To adopt a simulated threshold level to an experimental TSEM image the signal levels of the simulation have to be related to the grey scale values of the image as depicted in figure 7. For every single particle present in the image these grey values are individually deduced from the so-called regions of interest (ROIs) which are individually defined in the vicinity of the particles. The grey value g_1 (corresponding to S_1 in the simulation) is determined as the median grey scale value of the background of a ROI. The grey value g_0 (corresponding to S_0) is determined as the mean grey value of a small amount of pixels centred at the object's centre of mass. Using these data the desired grey value threshold level g_{thres} is easily calculated according to the rule of three, see figure 7:

$$g_{\text{thres}}(d) = \frac{S_{\text{thres}}(d) - S_0(d)}{S_1 - S_0(d)} \cdot (g_1 - g_0) + g_0.$$

In this equation, the dependence of the simulated signals on the particle diameter d is explicitly stated. One should note that not only the threshold signal level S_{thres} but also the signal level S_0 at the centre of the particle depends on particle size; the thicker the particle the lower S_0.

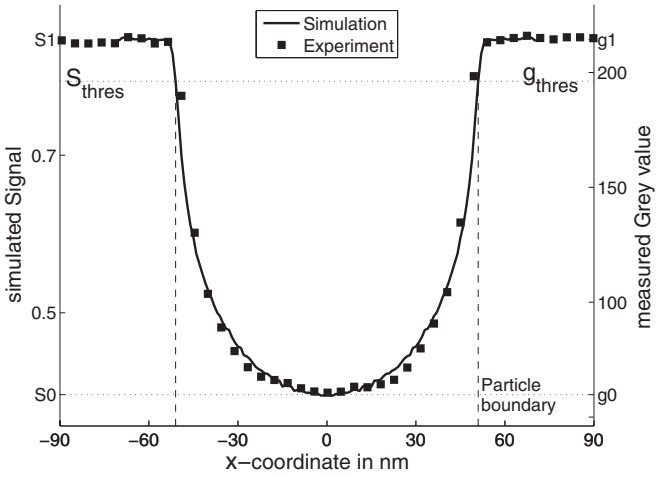

Figure 7. Simulated TSEM signal profile across a latex sphere together with a corresponding measured grey scale profile (converted to 8 bit for better readability).

4. Analysis of the TSEM images of nanoparticles

In order to analyse the recorded TSEM images, a Matlab [13] program has been developed which makes use of some powerful particle analysing routines of the open source image analysis software ImageJ [14]. Not yet optimized for speed, the program already enables the analysis of thousands of particles in hundreds of images in less than an hour.

The boundary of every particle is determined individually. For this purpose, we apply the threshold level that is predicted by the simulation of a particle of corresponding size and material. Since the threshold level depends on particle size which is not known initially, we employ an iterative procedure. For a first guess a global thresholding technique is used, the so-called minimum or mode algorithm [15]. It gives a first estimate of the particle size, which in turn is used to calculate an improved threshold level leading to an improved estimate of the particle size and so forth. The procedure stops when the threshold level and particle size remain stable which usually takes less than ten iterations.

For the determination of the particle boundary the final threshold level derived by the iterative procedure is applied. In order to reduce digitization errors the particle boundary is determined with sub-pixel accuracy. For this purpose, the ROI containing the particle is interpolated by a factor of 5 in both x and y directions, i.e. the image size becomes 25-fold larger. After the individual thresholding the number of sub-pixels belonging to the particle are counted and multiplied with the area (in nm^2) of a single sub-pixel. The final particle size is defined as the diameter of a sphere exhibiting the same projected area.

In order to distinguish isolated nanoparticles from particle clusters and artefacts, such as e.g. impurities, objects which do not fit within a certain size range or which possess a circularity smaller than a certain minimum are rejected. However, this relatively simple approach entails the risk of missing actual particles with extreme size or shape and of including artefacts that are similar to actual particles. A precise tuning of three parameters (minimal and maximum sizes as well as circularity) is therefore necessary. To reduce inclusion of artefacts, the best strategy is using pure samples and a sound sample preparation under clean room conditions.

Although there are useful methods available for a variety of applications [16], no attempt is made to separate and measure touching particles. Even after successful segmentation of touching or overlapping particles their size may either be underestimated or restoring their original shape relies on assumptions which may not be adequate for highly accurate traceable measurements.

5. Measurement uncertainty

For the evaluation of the uncertainty associated with the measurement of the mean particle size we applied the internationally accepted rules described in the '*Guide to the Expression of Uncertainty in Measurement*' (GUM) [17]. In the following we discuss input quantities which are relevant for the measurement uncertainty.

The calibration of the length scale of the SEM instrument is described in section 2 together with the effects that influence the pixel size. These effects have to be considered together with the uncertainty of the calibration standard in order to determine the uncertainty associated with the obtained pixel size. It turns out that the resulting uncertainty contribution to the nanoparticle size plays only a minor role compared with the other uncertainty components discussed below.

The uncertainty of the simulated threshold signal level S_{thres} is an important contribution to the uncertainty budget of the mean size because it directly determines the position of the particle boundary and thus the particle size. There is an uncertainty attributed to the simulated threshold level because the relevant input quantities discussed in section 3 cannot be determined exactly. Furthermore only a limited number of electrons can be used for the simulations and there are uncertainties associated with the electron scattering cross-sections and the density of the materials involved. Also some assumptions like that of spherical particles are only approximately valid. All these contributions need to be considered to estimate the resulting uncertainty of the threshold signal level S_{thres}.

As an example, we discuss here in greater detail the influence of the electron beam width because it is considered to have a major impact on the uncertainty attributed to the simulated threshold level. From the TSEM images of gold particles taken with an almost perfectly adjusted SEM an electron beam width (full width at half maximum, FWHM) of 3 nm could be deduced. The typical FWHM present during automated image acquisition, which involves moving the sample stage, is supposed to be somewhat worse. Images taken with a FWHM of 8 nm (made by intentional misalignment of the beam focus) are readily recognized as misaligned and are hardly evaluable. From these observations the lower and upper limits of the beam width are estimated to be 3 nm and 8 nm, respectively, while the average beam width is assumed to be 5 nm. Consequently, simulations were performed for these three beam sizes resulting in a threshold signal level

used for the image evaluations (i.e. the one obtained for 5 nm FWHM) and an uncertainty of the threshold level derived from the deviations obtained for the smaller and larger electron beam sizes.

Other important uncertainty contributions arise from the analysis of the recorded TSEM images. For instance, there is an uncertainty associated with the determination of the background grey value g_1 and the grey value g_0 in the centre of a particle. The determination of g_0 and g_1 is influenced by image noise and further effects such as, e.g., unwanted additional TSEM signals caused by inhomogeneities of the carbon support film or possibly dried-up residuals of the dispersion liquid.

Image noise present at the particle boundary is not that important. Some pixels lying at or near the particle boundary may show grey values that are randomly above or below the threshold level leading to erroneous inclusion or exclusion of pixels. The expected value of the resulting deviation in particle size is zero and a detailed analysis shows that the corresponding uncertainty can be neglected in comparison to other uncertainty components.

To sort out agglomerates and artefacts such as dirt, we use three intuitive geometric parameters as criteria: minimum and maximum particle sizes as well as minimum circularity. The choice has to be done manually but the software provides assistance. For instance, in the case of latex particles the minimum circularity is chosen to be quite high because latex particles are considered to be almost spherical. In contrast, gold nanoparticles which may show facets require a smaller value of the minimum circularity. However, even a careful choice entails the risk of missing actual particles and including artefacts. To estimate the effect of varying parameters the image analysis is carried out not only for the best guess values but also for hardly justifiable but still realistic extreme values. Using the extreme values the number of objects which are included in the analysis changes. Consequently the size distributions and possibly also the mean particle size are altered and the corresponding uncertainty of the mean particle size can be estimated.

Because circular objects are represented in a digital image as a number of square pixels, digitization errors occur. The resultant uncertainty contribution is reduced considerably by interpolating the original image before determining the size.

A reasonable number of particles has to be analysed in order to get statistically meaningful results. No assumptions for the particle size distribution are made and hence the associated statistical uncertainty component is determined by the experimental standard deviation of the sample mean. (Presupposing a log-normal size distribution the statistical uncertainty of the mean particle size could be estimated to lower values [18].) Since a sufficient number of particles (some thousands) has been analysed and since the particle size distributions are comparably narrow, the statistical uncertainty portion is small compared to the combined effect of the systematic uncertainty contributions.

Sample preparation should guarantee that a representative subsample of the suspended particles is present on the substrate. An ongoing research project addresses this question [19]. For the time being an uncertainty contribution, due to possibly imperfect sample preparation, is not included in the uncertainty budget. The stated data such as the spread of the size distribution and its mean value describe the nanoparticles present on the substrate.

Table 1. Measurement results for the three nanoparticle samples under test.

	Gold	Silica	Latex
Mean particle size (nm)	9.1	27.5	44.5
Expanded uncertainty of the mean size (nm)	1.2	1.7	2.6
Statistical standard deviation of the sample mean size (nm)	0.02	0.09	0.17
Spread of size distribution (nm) (standard deviation of the particle size)	0.8	5.2	7.9
Median size (nm)	9.1	28.9	45.7
Mode size (nm)	9.1	29.6	46.7
Number of TSEM images taken	266	230	271
Number of analysed particles	2318	3144	2113

Quadratic summation of all uncertainty contributions yields the combined uncertainty from which the expanded measurement uncertainty of the mean particle size is derived (coverage factor $k = 2$, i.e. 95% confidence interval). For the three nanoparticle samples studied here, the expanded uncertainties are in the range of 1 to 3 nm, see table 1. One should emphasize that these expanded uncertainties contain all known uncertainty contributions including the relatively small statistical component. This should be kept in mind when comparing these uncertainty values with other published data which sometimes state only the statistical uncertainty component.

6. Results and discussion

In this section the results of the measurements of the three nanoparticle samples under test are presented and discussed. Table 1 summarizes the measured data. It contains the mean particle size and its associated expanded uncertainty, data characterizing the size distribution and the number of images taken and particles analysed.

A typical TSEM image of the gold nanoparticles is shown in figure 8 together with the resulting size distribution based on an analysis of about 2300 individual particles. The mean particle size is 9.1 nm with an expanded uncertainty of 1.2 nm. In the accompanying 'Report of Investigation' from the National Institute of Standards and Technology (NIST) a mean diameter measured by TEM of 8.9 nm is given [20]. The expanded uncertainty of 0.1 nm stated therein is based on twice the standard deviation of replicate measurements. Hence, the mean particle size measured in this study is in agreement with the NIST data. The different uncertainties are partly due to the fact that the expanded uncertainty stated here also includes the dominant systematic uncertainty contributions. As can be seen in figure 9 the size distribution measured in this work and the size distribution presented in the NIST report differ slightly. Besides an offset comparable to the variation of the mean sizes,

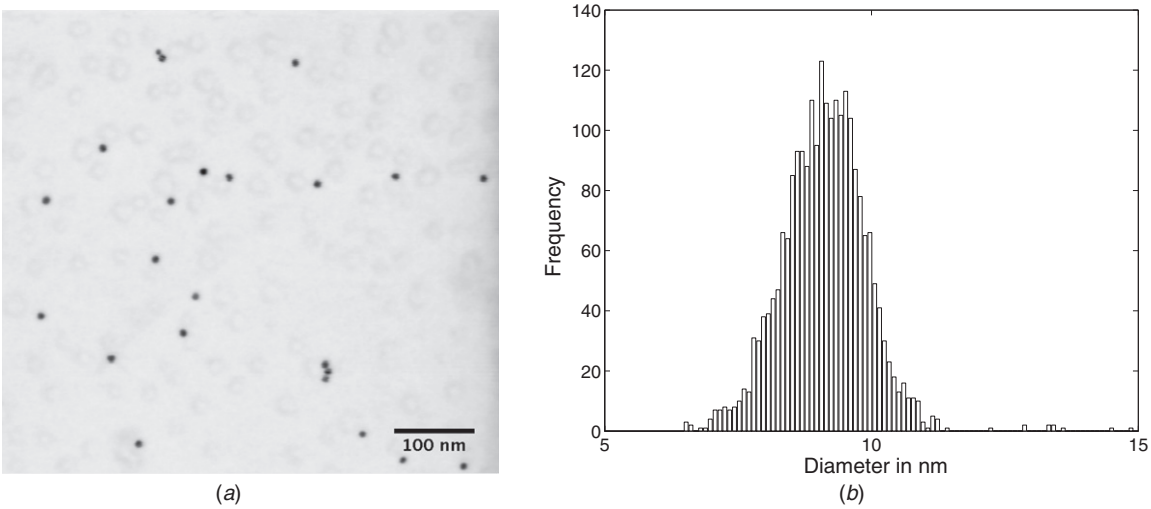

Figure 8. TSEM image of gold nanoparticles (*a*) together with the size distribution (*b*).

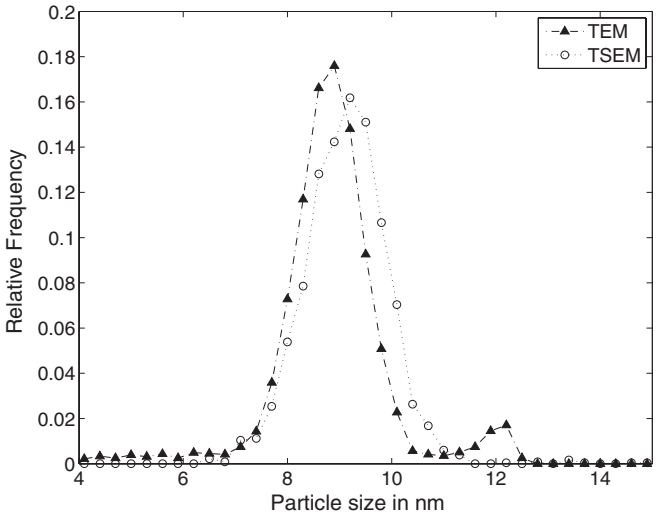

Figure 9. Size distribution of gold nanoparticles as measured with TEM (NIST) and TSEM, respectively.

a fraction of larger particles (about 12 nm) is present only in the TEM measurement. This may be an issue of statistics or subsampling.

One may conclude that TSEM and TEM measurements lead to comparable results in measuring nanoparticle size. Since the operation of a TEM is expensive, difficult and time consuming compared to working with an SEM, TSEM may be used if the highest resolution and measurement of very small nanoparticles below about 5 nm are not that important.

The measurement of the silica particles revealed a small bimodality of the size distribution (see figure 10). Since more than 3100 particles were analysed, the bimodality is statistically significant. This example makes obvious a relevant advantage of imaging techniques with respect to ensemble measurements such as DLS etc: although ensemble techniques are much faster than automated electron microscopy, it is very hard to resolve and quantify such small bimodalities [21].

Figure 11 shows the size distribution of the measured latex particles. The size histogram shows a significant deviation from regular distributions such as normal or log-normal distributions. Again such unusual distributions are hard to resolve using ensemble measurement techniques.

7. Conclusion and outlook

The feasibility of the TSEM technique for traceable measurements of nanoparticles down to about 5 nm has been demonstrated for three different material classes. Accurate size measurement relies on accurate detection of the particle boundary which can be improved using physical models to simulate image formation. As a result of these simulations, the obtained threshold signal used to determine the particle boundary in the image depends on the material and size of the particle. Consequently, an iteration procedure is necessary during image analysis to adapt the threshold level for every single particle under test. Despite this effort, a thorough characterization of a sample can be achieved surprisingly fast by means of automated image acquisition as well as automated analysis of some thousand particles overcoming the drawback of insufficient statistics often associated with electron microscopy. By this approach, expanded uncertainties of about 1 to 3 nm for the mean particle size are achievable with commercially available instrumentation. However the uncertainty attributed to sample preparation is not included in the stated values.

Future work will be done to improve the versatility of the TSEM technique. Soon a possibility to analyse non-spherical particles such as nanorods will be implemented in the image analysis software. Expanding the application range of TSEM to low-*Z* materials, contrast optimization will play an important role; hence studies on varying electron energy and detector acceptance angle will be worthwhile. In this context receiving thickness information is conceivable as was demonstrated by Barkay *et al* [22]. The possibility of simulating dark-field images has already been shown [3] and there will be an evaluation of possible advantages of this mode. Eventually the contribution of sample preparation, i.e. the question of representativity of the measured sample, is studied

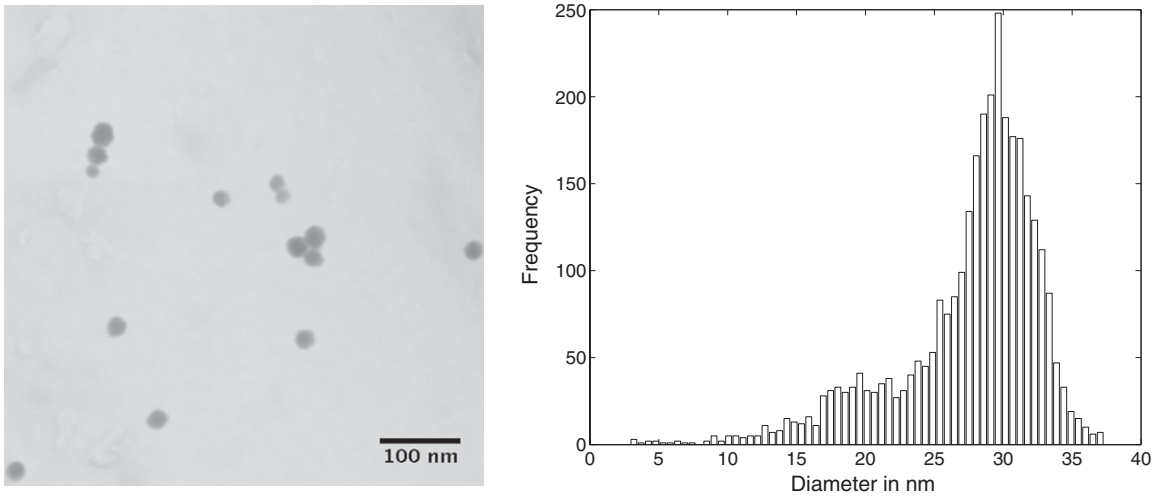

(*a*) (*b*)

Figure 10. TSEM image of silica nanoparticles (*a*) together with the size distribution (*b*).

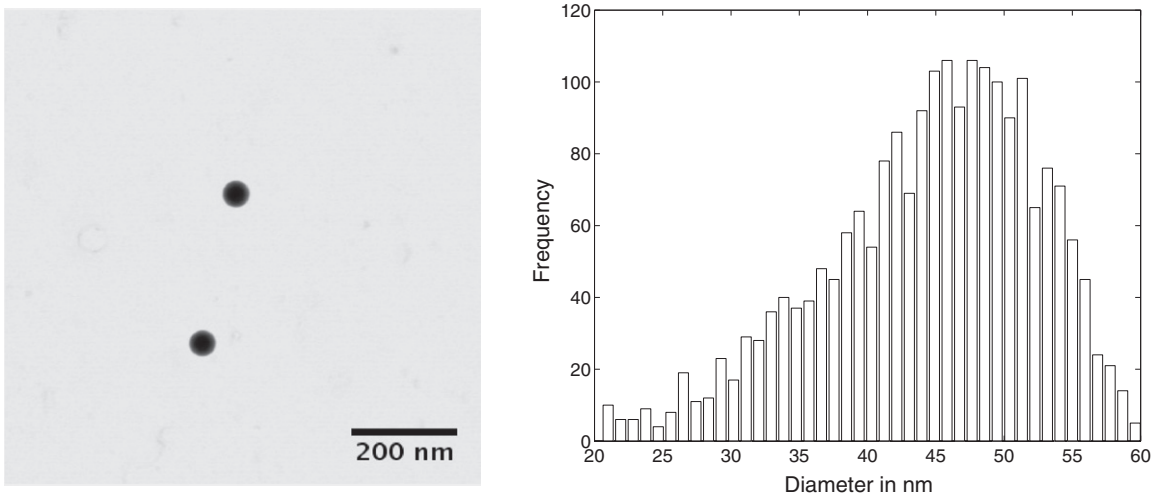

(*a*) (*b*)

Figure 11. TSEM image of latex nanospheres (*a*) together with the size distribution (*b*).

at the moment in order to accomplish a thorough uncertainty analysis.

Acknowledgments

The authors would like to thank Dominic Gnieser for his contributions in the development of MCSEM and Vincent Hackley for sharing the NIST data. The European Commission funded this work through the grant EMRP T3.J1.1 'Traceable characterization of nanoparticles'.

References

[1] Van Ngo V, Hernandez M, Roth B and Joy D C 2007 STEM imaging of lattice fringes and beyond in a UHR in-lens field-emission SEM *Microsc. Today* **15** 12–6

[2] Farrow R C *et al* 1997 Application of transmission electron detection to SCALPEL mask metrology *J. Vac. Sci. Technol.* B **15** 2167–72

[3] Buhr E, Senftleben N, Klein T, Bergmann D, Gnieser D and Frase C G 2009 Characterization of nanoparticles by scanning electron microscopy in transmission mode *Meas. Sci. Technol.* **20** 084025

[4] Postek M T, Lowney J R, Vladar A E, Keery W J, Marx E and Larrabee R D 1993 X-ray lithography mask metrology: use of transmitted electrons in an SEM for linewidth measurement *J. Res. Nat. Inst. Stand. Technol.* **98** 415–45

[5] Buhr E, Michaelis W, Diener A and Mirandé W 2007 Multi-wavelength VIS/UV optical diffractometer for high-accuracy calibration of nano-scale pitch standards *Meas. Sci. Technol.* **18** 667–74

[6] Chernoff D A, Buhr E, Burkhead D L and Diener A 2008 Picometer-scale accuracy in pitch metrology by optical diffraction and atomic force microscopy *Proc. SPIE* **6922** 69223J

[7] Sezgin M and Sankur B 2004 Survey over image thresholding techniques and quantitative performance evaluation *J. Electron. Imaging* **13** 146–68

[8] Sadowski T E, Broadbridge C C and Daponte J 2007 Comparison of common segmentation techniques applied to

transmission electron microscopy images *Mater. Res. Soc. Symp. Proc.* **982** 25–30
[9] Frase C G, Gnieser D and Bosse H 2009 Model-based SEM for dimensional metrology tasks in semiconductor and mask industry *J. Phys. D: Appl. Phys.* **42** 183001
[10] Johnsen K P, Frase C G, Bosse H and Gnieser D 2010 SEM image modeling using the modular Monte Carlo model MCSEM *Proc. SPIE* **7638** 76381O
[11] Salvat F and Mayol R 1993 Elastic scattering of electrons and positrons by atoms. Schrödinger and Dirac partial wave analysis *Comput. Phys. Commun.* **74** 358–74
[12] Joy D C and Luo S 1989 An empirical stopping power relationship for low-energy electrons *Scanning* **11** 176–80
[13] 2009 *MATLAB R2009a* (Natick, MA: The MathWorks Inc.)
[14] Abramoff M D, Magelhaes P J and Ram S J 2004 Image processing with ImageJ *Biophotonics Int.* **11** 36–43
[15] Prewitt J M and Mendelsohn M L 1965 The analysis of cell images *Ann. NY Acad. Sci.* **128** 1035–53
[16] Vincent L and Soille P 1991 Watersheds in digital spaces: an efficient algorithm based on immersion simulations *IEEE Trans. Pattern Anal. Mach. Intell.* **13** 583–98
[17] ISO 1993 *Guide to the Expression of Uncertainty in Measurement* (Geneva: International Organization for Standardization)
[18] ISO 2004 Particle size analysis—image analysis methods: part 1. Static image analysis methods *ISO 13322-1* (Geneva: International Organization for Standardization)
[19] DIN INS Präparationsmethoden für Größenmessungen—Realisierung und Optimierung von Präparationsmethoden für zuverlässige Größenmessungen mit AFM und TSEM (Preparation techniques for size measurements)
[20] Kaiser D L and Watters R L 2007 *Reference Material 8011, Report of Investigation* (Gaithersburg, MD: National Institute of Standards and Technology)
[21] Rasteiro M G, Lemos C C and Vasquez A 2008 Nanoparticle characterization by PCS: the analysis of bimodal distributions *Part. Sci. Technol.* **26** 413–37
[22] Barkay Z, Rivkin I and Margalit R 2009 Three-dimensional characterization of drug-encapsulating particles using STEM detector in FEG-SEM *Micron* **40** 480–5